



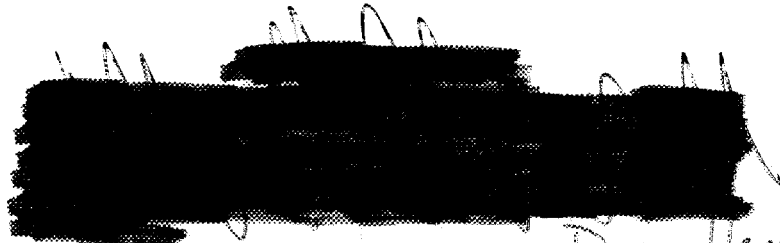
3 4456 0451814 5

973



# Multiaxial Low-Cycle Fatigue of Type 304 Stainless Steel

J. J. Blass  
S. Y. Zamrik



NO LONGER AT Dave Hamish 9/3/01

OAK RIDGE NATIONAL LABORATORY  
CENTRAL RESEARCH LIBRARY  
CIRCULATION SECTION  
3500N ROOM 173

## LIBRARY LOAN COPY

DO NOT TRANSFER TO ANOTHER PERSON  
if you wish someone else to see this report, send in name with report and the library will arrange a loan

ORNL-118 (6-67)

CS 3-601

# OAK RIDGE NATIONAL LABORATORY

OPERATED BY UNION CARBIDE CORPORATION FOR THE ENERGY RESEARCH AND DEVELOPMENT ADMINISTRATION



ORNL/TM-5609  
Dist. Category  
UC-79, -79e, -79h, -79k

Contract No. W-7405-eng-26

Engineering Technology Division

MULTIAXIAL LOW-CYCLE FATIGUE OF TYPE 304 STAINLESS STEEL

J. J. Blass  
Oak Ridge National Laboratory

S. Y. Zamrik  
The Pennsylvania State University

Date Published: October 1976

LOCKHEED MARTIN ENERGY RESEARCH LIBRARIES



3 4456 0451814 5

OAK RIDGE NATIONAL LABORATORY  
Oak Ridge, Tennessee 37830  
operated by  
UNION CARBIDE CORPORATION  
for the  
ENERGY RESEARCH AND DEVELOPMENT ADMINISTRATION



## CONTENTS

	<u>Page</u>
ABSTRACT .....	1
INTRODUCTION .....	1
SPECIMENS, MATERIAL, AND TEST METHODS .....	2
TEST RESULTS AND CORRELATIONS .....	3
EQUIVALENT STRAIN .....	11
PLANE OF MAXIMUM SHEAR STRAIN .....	22
CUMULATIVE DAMAGE .....	26
SUMMARY AND CONCLUSIONS .....	28
ACKNOWLEDGMENT .....	29
REFERENCES .....	30



## MULTIAXIAL LOW-CYCLE FATIGUE OF TYPE 304 STAINLESS STEEL

J. J. Blass  
Oak Ridge National Laboratory

S. Y. Zamrik  
The Pennsylvania State University

### ABSTRACT

Tubular specimens of type 304 stainless steel were subjected to simultaneous push-pull and alternating twist at room temperature, 538°C (1000°F), and 649°C (1200°F). Six ratios of shear strain to axial strain were employed. Tests with a step change in strain range were performed, as well as constant strain range tests. In the step tests, high-low and low-high sequences of straining and several ratios of applied cycles to estimated cycles to failure were employed. Data correlations based on the method of least squares were developed to aid in the interpretation of trends. The results indicate that a failure criterion based on the shear and normal strains on the plane of maximum shear strain would be more effective than those based on equivalent strain and other traditional measures. The results also indicate that multi-axial loading is not significantly different from uniaxial loading with regard to the effectiveness of a linear cumulative damage law.

### INTRODUCTION

Examples of current structural design methods may be found in Case 1592-7 of the ASME Boiler and Pressure Vessel Code<sup>1</sup> which contains rules for elevated temperature design of nuclear power plant components. For fatigue, the rules are based on a definition of equivalent strain range, a linear cumulative damage law, and curves or tabular data relating total strain range to design allowable cycles. This report examines these methods in light of a limited amount of test data<sup>2</sup> for type 304 stainless steel at room and elevated temperatures. The data were obtained from completely reversed combined extension and twist experiments on tubular specimens with the ratio of twist to extension held

constant in each experiment. The experiments were conducted in the second author's laboratory at Pennsylvania State University as a part of Oak Ridge National Laboratory's High-Temperature Structural Design Program.

#### SPECIMENS, MATERIAL, AND TEST METHODS

The tubular test specimens,<sup>2</sup> which had a wall thickness of 1.5 mm (0.060 in.), an outside diameter to wall thickness ratio of about 8, and an effective gage length of about 28 mm (1.1 in.), were made from 25 mm (1 in.) hot rolled bar of the well characterized<sup>3,4</sup> U.S. Energy Research and Development Administration (ERDA) reference heat (9T2796) of type 304 stainless steel. They were annealed at 1093°C (2000°F) for 30 min in argon, after machining and honing. The experiments were conducted in a horizontal hydraulic testing machine capable of independent electronic servocontrol of axial force and torsional moment or of axial and torsional relative displacements.

Because of the difficulties associated with dynamic multiaxial strain measurements at elevated temperature, the electrical outputs of LVDT and RVDT\* displacement transducers mounted on the machine's linear and rotary hydraulic actuators were used for indirect control of axial strain and engineering shear strain over the reduced section of the specimen. These transducers were calibrated at room temperature under monotonic loading against high-elongation electrical resistance strain gage rosettes bonded to the outside surface of the reduced section of the specimen. Results of several calibration runs showed a high degree of repeatability. Additional checks were made to verify that the relationship between the outputs of the actuator mounted transducers and the motion of the specimen grips was relatively insensitive to axial load, torque, and temperature.

In these experiments a common 0.42 Hz (25 cpm) sinusoidal signal was used as input to both axial and torsional control systems so that

---

\*Linear variable differential transformer and rotary variable differential transformer.

the ratio,  $R$ , of engineering shear strain to axial strain was held constant in each test. Because of the sinusoidal wave form the strain rate varied continuously in each cycle. The average equivalent strain rate, defined as twice the product of equivalent strain range and frequency, varied from 0.0029 to 0.052  $\text{sec}^{-1}$  (a factor of 18) depending on strain range.

In the elevated temperature tests each specimen was heated internally by means of a silicon carbide resistance heating element in the form of a 6.4 mm (0.25 in.) diameter rod, 171 mm (6.75 in.) long, with a central heated length of approximately 44 mm (1.75 in.). The element was positioned along the axis of the specimen so as to equalize the temperatures at both ends of the reduced section and was free to expand and contract. Two chromel-alumel thermocouples, spot welded to the outside surface of the specimen, were used for automatic temperature control.

#### TEST RESULTS AND CORRELATIONS

The results of 84 constant strain range experiments at room temperature, 538°C (1000°F), and 649°C (1200°F), with the ratio,  $R$ , of engineering shear strain to axial strain equal to 0, 1/2, 1, 2, 5, and  $\infty$ , are listed in Table 1. The results of 45 experiments conducted under a sequence of two constant strain ranges at the same temperatures, and with  $R = 0, 1/2, 1, \text{ and } 2$ , are listed in Table 2.

For the purpose of accurate interpolation among data points and to aid in the interpretation of data trends, the total strain range vs cycles to failure data of Table 1 were modeled by a two-term power law, after the uniaxial observations of Basquin,<sup>5</sup> Coffin,<sup>6,7</sup> Manson,<sup>8,9</sup> and Morrow.<sup>10</sup> For pure tension,  $R = 0$ , this relationship takes the form

$$\Delta\epsilon_z = a_3 N_f^{a_1} + a_4 N_f^{a_2}, \quad (1)$$

where  $\Delta\epsilon_z$  is the axial strain range. For pure torsion,  $R = \infty$ ,  $\Delta\epsilon_z$  in Eq. (1) was replaced by the engineering shear strain range,  $\Delta\gamma_{\theta z}$ . For other values of  $R$ , Eq. (1) was used in conjunction with  $\Delta\gamma_{\theta z} = R \Delta\epsilon_z$ .

Table 1. Constant strain range multiaxial fatigue tests of annealed type 304 stainless steel (heat 9T2796)

0		1/2		1		2		5		$\infty$	
$\Delta\epsilon_z$ (%)	$N_f$ (Cycles)	$\Delta\epsilon_z$ (%)	$N_f$ (Cycles)	$\Delta\epsilon_z$ (%)	$N_f$ (Cycles)	$\Delta\epsilon_z$ (%)	$N_f$ (Cycles)	$\Delta\epsilon_z$ (%)	$N_f$ (Cycles)	$\Delta\gamma_{\theta z}$ (%)	$N_f$ (Cycles)
R = $\Delta\gamma_{\theta z} / \Delta\epsilon_z$											
[Room Temperature]											
3.70	230	2.00	1,075	2.00	1,160	1.00	2,484	1.00	1,100	10.80	425
2.80	700					1.00	2,780				
2.00	1,268	1.50	1,700	0.80	4,100	0.75	4,300			4.32	3,130
1.40	2,000					0.60	6,000				
1.00	3,170	0.50	11,550			0.50	6,900			2.84	7,715
0.90	3,728										
0.60	9,765									2.16	12,655
0.55	12,050										
[538°C (1000°F)]											
3.00	172	1.60	680	1.20	835	1.00	1,008			4.32	1,000
1.50	608	1.20	1,187	1.00	955	0.60	2,425			3.60	1,438
0.75	2,426	0.70	2,200	0.80	1,698	0.50	3,333			2.00	4,850
0.50	5,750	0.60	2,873	0.60	3,178	0.40	7,047			1.58	7,800
0.40	8,733	0.40	5,398	0.30	10,050	0.30	11,068			1.08	17,600
0.35	12,411										
[649°C (1200°F)]											
2.70	75	1.20	110	0.72	100	0.75	400	0.60	215	7.20	230
3.00	145			0.90	152	0.60	693				
2.00	175	1.50	150	1.304	200	0.60	800	0.20	6,200	4.32	585
1.80	230			0.60	700	0.50	830				
1.10	563	0.80	164	0.70	865	0.40	2,612			2.16	2,060
1.00	600			0.40	1,121	0.30	4,045				
1.00	630	0.60	1,074	0.40	2,390	0.28	7,800			1.44	5,234
0.70	1,510					0.25	12,800				
0.50	5,552	0.50	2,452								

Table 2. Multiaxial fatigue tests with a step change in strain range  
annealed type 304 stainless steel (heat 9T2796)

[Room Temperature]			[538°C (1000°F)]							
$R = \Delta\gamma_{\theta z} / \Delta\epsilon_z$	2		$R = \Delta\gamma_{\theta z} / \Delta\epsilon_z$		1		2		2	
$\Delta\epsilon_z$ (%)	1.00	0.50	1.304	0.652	1.00	0.50	0.50	1.00		
$N_f$ (cycles)	2659	7471	683	2404	935	3795	3795	935		
$N_f$ (cycles)	2237	11842	614	2371	1037	3295	3295	1037		
	$n_1$	$n_2$	$n_1$	$n_2$	$n_1$	$n_2$	$n_1$	$n_2$	$n_1$	$n_2$
	(cycles)	(cycles)	(cycles)	(cycles)	(cycles)	(cycles)	(cycles)	(cycles)	(cycles)	(cycles)
	278	12500	70	2195	100	2960	668	915		
	556	7040	210	1542	300	2100	1336	750		
	1112	5038	280	1220	400	1730	2004	586		
	1668	2962	420	650	600	970	2672	380		
	2224	760	630	30	700	525				
					900	100				

[649°C (1200°F)]										
$R = \Delta\gamma_{\theta z} / \Delta\epsilon_z$	0		1/2		1		2		2	
$\Delta\epsilon_z$ (%)	1.50	0.75	1.442	0.721	1.304	0.652	1.00	0.50	0.50	1.00
$N_f$ (cycles)	311	1473	66.3	615	39.0	511	175	1148	1148	175
$N_f$ (cycles)	215	844	79.8	665	160	772	266	1238	1238	266
	$n_1$	$n_2$								
	(cycles)									
	46	682	10	590	20	686	30	1385	200	250
			20	500	60	487	60	728		
	112	415	40	330	100	265	120	492	400	220
			60	135	140	77	180	241		
	168	110	80	20	160	30	210	110	700	144
							240	48		
	224	15					270	20	800	100

NOTE: This table lists the numbers of cycles,  $n_1$  and  $n_2$ , for which each of two values of axial strain range,  $\Delta\epsilon_z$ , were applied in combination with the engineering shear strain range defined by the ratio  $R$ . Two values of the corresponding number of cycles to failure,  $N_f$ , under constant strain range conditions are shown. The first was calculated from Eq. (1) fitted to the constant strain range data of Table 1 and the second from Eq. (7) fitted to the  $n_2$  vs  $n_1$  data of this table by the method of least squares.

The exponents  $a_1$  and  $a_2$  (both negative) were taken to depend on temperature, and the coefficients  $a_3$  and  $a_4$  (both positive) were taken to depend on temperature and the ratio  $R$ .

The fitting was done to log-log coordinates, just as such data are usually plotted, using a least squares criterion of fit. Mathematically this means that the values of the elements of the array  $\underline{a} = (a_1, \dots, a_{2+2m})$  were chosen to minimize, at each temperature, the unexplained variation

$$V(\underline{a}) = \sum_{j=1}^m \sum_{i=1}^{n_j} [\log \Delta \epsilon_i - \log(a_{1+2j} N_i^{a_1} + a_{2+2j} N_i^{a_2})]^2, \quad (2)$$

where  $n_j$  is the number of data points,  $\Delta \epsilon_i$  vs  $N_i$ , for the  $j$ th value of  $R$  and  $m$  is the number of  $R$  values. The short computer program written to accomplish this fitting process made use of a general purpose subroutine<sup>11</sup> for finding the minimum of the sum of squares of  $M$  functions in  $N$  variables by means of a finite difference Levenberg-Marquardt<sup>12</sup> algorithm.

The above fitting process was also carried out with the exponents  $a_1$  and  $a_2$  in Eq. (1) taken to be independent of temperature. In this case each value of  $j$  in Eq. (2) refers to a particular combination of temperature and  $R$  ratio and  $m$  to the total number of such combinations.

The values of the parameters in the above models are given in Table 3, together with values of the scatter factor, which is defined by

$$S.F. = \text{antilog } \sqrt{V_{\min} / (n_d - n_a)},$$

where  $V_{\min}$  is the minimum value of  $V$  in Eq. (2),  $n_d = \sum_{j=1}^m n_j$ , the total number of data points used in the fit, and  $n_a = 2+2m$ , the number of independent parameters. The significance of the above scatter factor is that for data which have a logarithmic normal distribution, 68% of the data can be expected to lie within this (multiplication or division) factor of the expected value of the dependent variable (here taken to be the axial or engineering shear strain range).

The strain range vs cycles to failure data of Table 1 are plotted in Figs. 1-4 to log-log coordinates. The solid-line curves in each

Table 3. Parameters in two-term power law [Eq. (1), with strain range in percent] representation of multiaxial low-cycle fatigue of annealed type 304 stainless steel (heat 9T2796)

	Room temperature		538°C (1000°F)		649°C (1200°F)	
	-0.42105	-0.67411	-0.37216	-0.68808	-0.26687	-0.75222
			Exponents			
			Coefficients			
$R = \Delta\gamma_{\theta z} / \Delta\epsilon_z$						
0	20.486	88.634	8.529	59.783	3.763	51.456
1/2	11.222	153.890	0.033	146.291	3.786	4.832
1	0.169	226.315	5.716	71.349	3.435	0.177
2	0.300	201.330	7.125	48.836	2.818	14.040
5					1.945	7.719
$\infty$	99.445	197.850	30.851	229.425	9.389	301.875
	1.107		Scatter factors 1.050		1.216	
	Temperature-independent exponents					
			-0.32825 -0.68220			
			Coefficients			
$R = \Delta\gamma_{\theta z} / \Delta\epsilon_z$						
0	8.862	107.496	5.388	66.266	5.998	30.636
1/2	5.421	159.401	0.242	144.250	5.906	0.035
1	0.566	229.126	3.607	74.907	5.009	0.094
2	0.779	202.860	4.623	52.353	5.134	0.004
5					3.506	0.001
$\infty$	46.818	198.067	20.653	229.607	7.272	290.786
			Scatter factor 1.162			

7

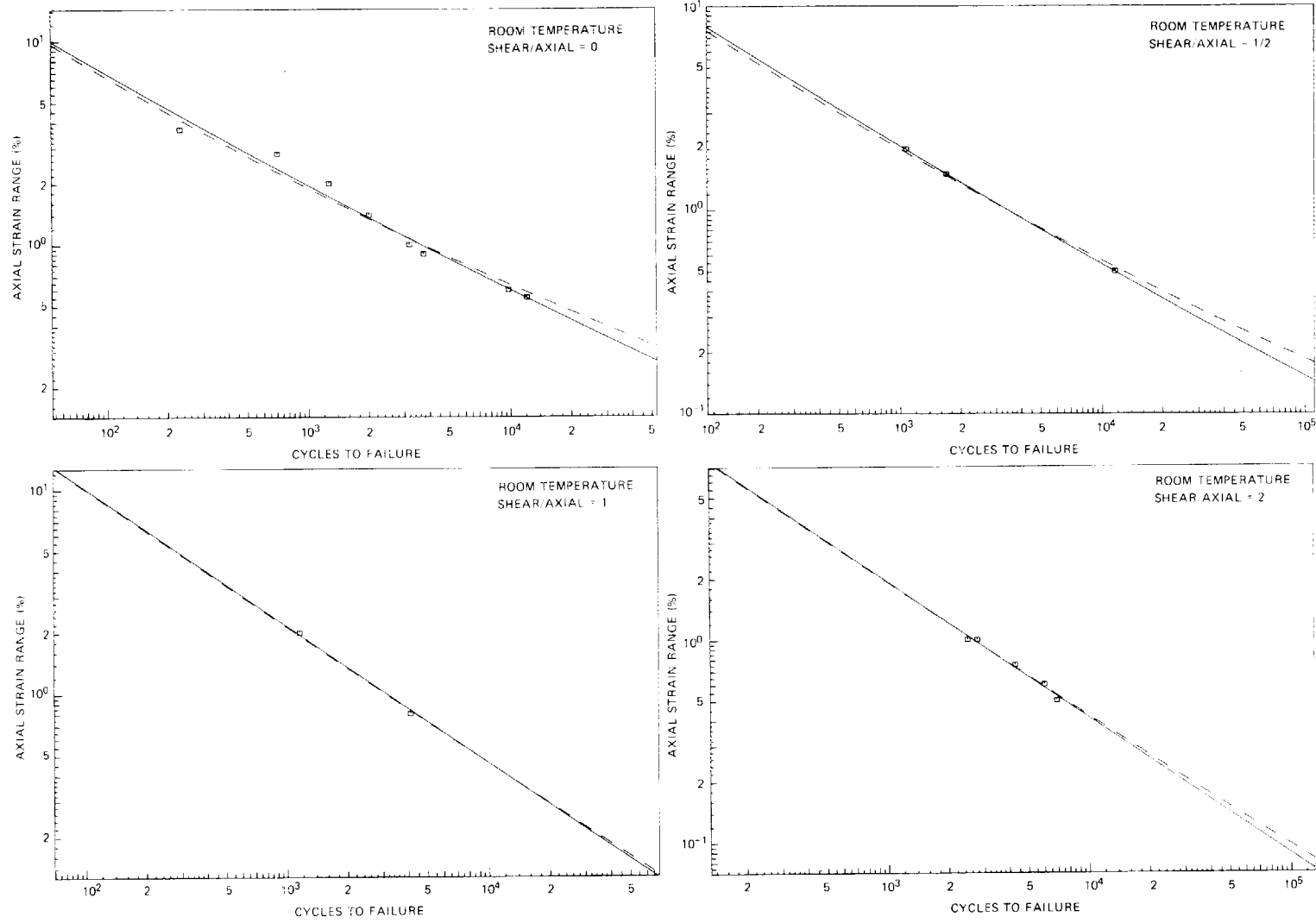


Fig. 1. Axial strain range vs cycles to failure in multiaxial low-cycle fatigue tests on annealed type 304 stainless steel (heat 9T2796).

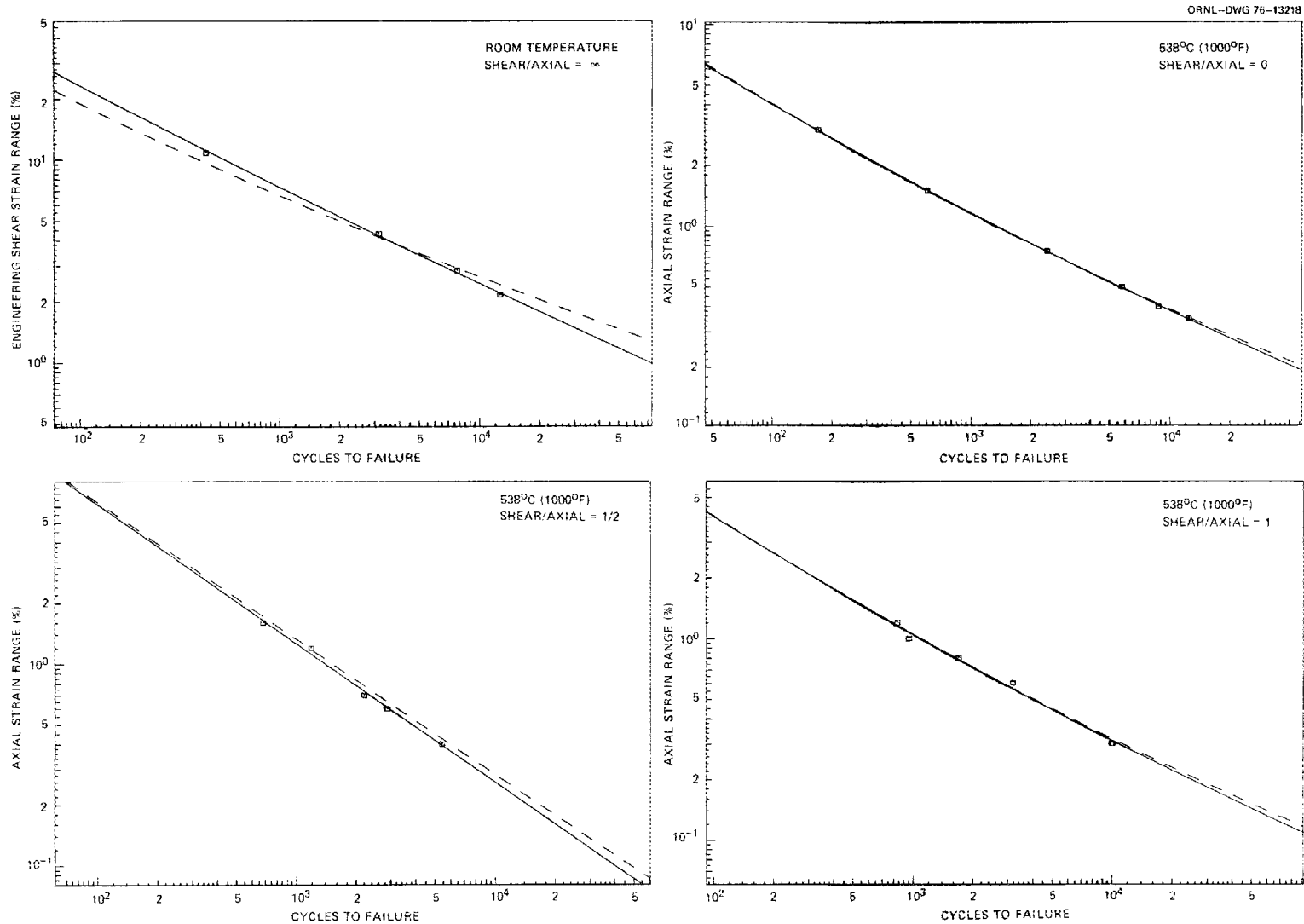


Fig. 2. Axial or engineering shear strain range vs cycles to failure in multiaxial low-cycle fatigue tests on annealed type 304 stainless steel (heat 9T2796).

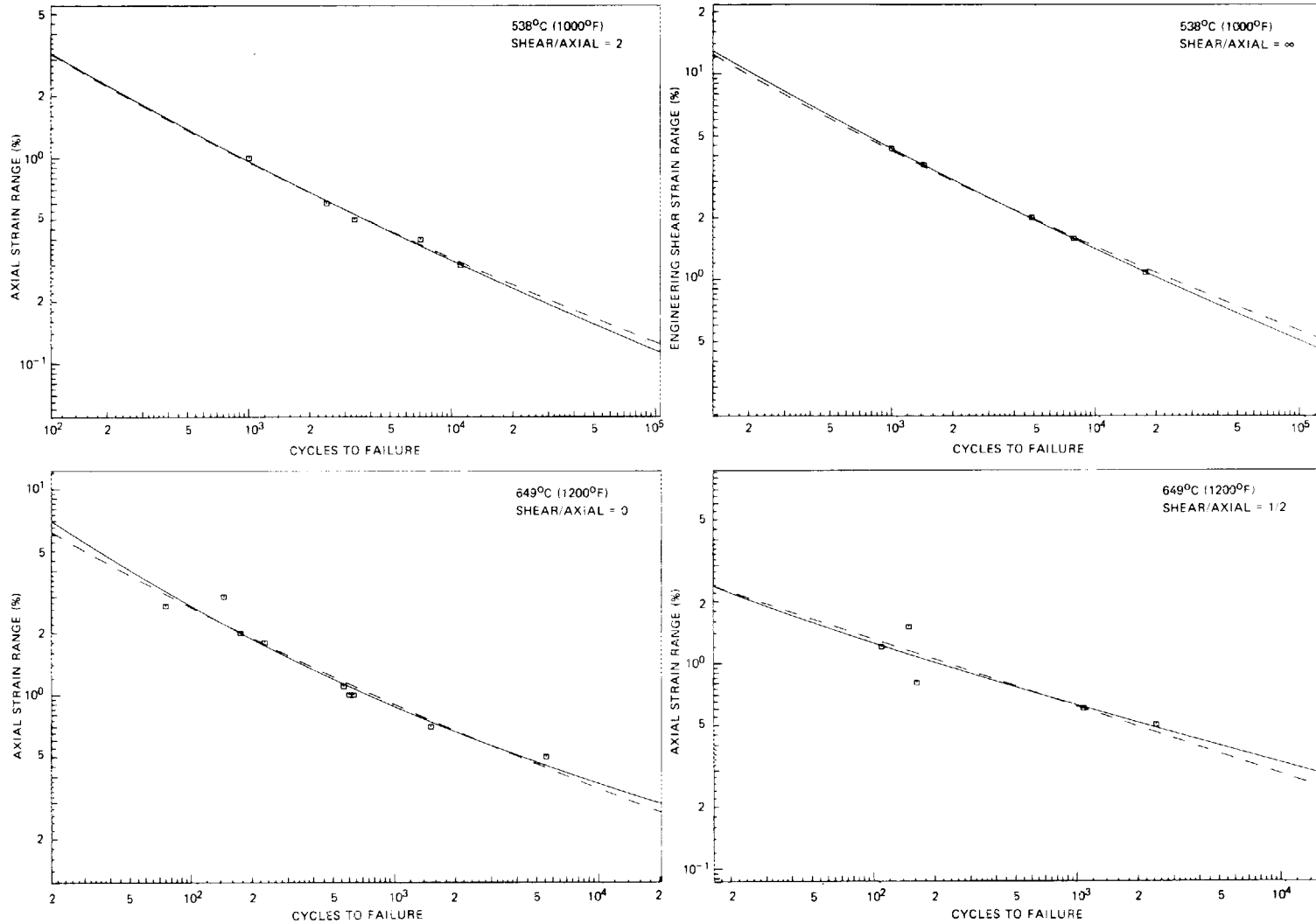


Fig. 3. Axial or engineering shear strain range vs cycles to failure in multiaxial low-cycle fatigue tests on annealed type 304 stainless steel (heat 9T2796).

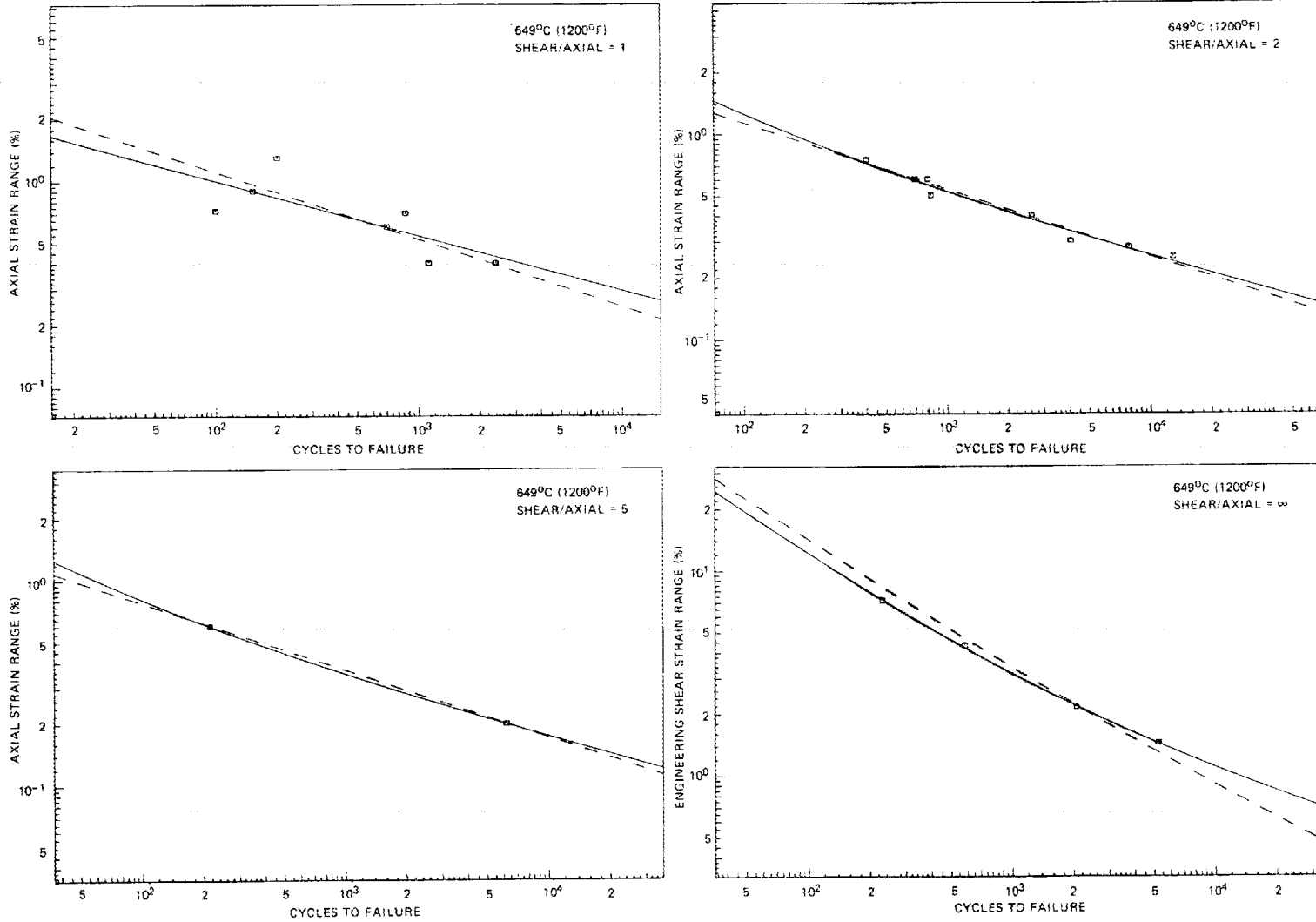


Fig. 4. Axial or engineering shear strain range vs cycles to failure in multi-axial low-cycle fatigue tests on annealed type 304 stainless steel (heat 9T2796).

figure represent the first model described above, with exponents dependent on temperature, and the dashed-line curves represent the second model, with exponents independent of temperature. The same scale is used for all figures, and the curves are extended to the boundaries, although they should not be regarded as accurate beyond the range of the data on which they are based.

The two-term power law form of Eq. (1) was also used by McAfee<sup>13</sup> to model the Code Case 1592-7 strain range,  $\epsilon_t = \Delta\epsilon_{\text{equiv}}$ , vs design allowable number of cycles,  $N_d$ , curves for type 304 stainless steel. The parameter values for the 38°C (100°F) curve and the 538°C (1000°F) to 649°C (1200°F) curve, at cyclic strain rates equal to or greater than 0.001 sec<sup>-1</sup>, which he obtained by means of least squares fits to log-log coordinates, are given in Table 4.

The Code design curves were constructed<sup>14</sup> by reducing curves fitted to available uniaxial low-cycle fatigue data<sup>15-20</sup> by a factor of 2 on total strain range or a factor of 20 on life, whichever results in a lower value of strain range. A reconstruction of the original (unreduced) fatigue curves in the form of Eq. (1) was obtained as follows. In Table T-1420-1A of Ref. 1 for the first seven entries at each temperature, with  $10 \leq N_d \leq 10^3$ ,  $N_d$  was multiplied by 20. For the last five entries, with  $4 \times 10^4 \leq N_d \leq 10^6$ ,  $\epsilon_t = \Delta\epsilon_{\text{equiv}}$  was multiplied by 2. The two-term power law of Eq. (1) was fitted to the transformed table entries in the manner described previously, with exponents taken to be both dependent on and independent of temperature. The resulting parameter values are given in Table 4.

Strizak<sup>21</sup> has also used the form of Eq. (1) to model uniaxial low-cycle fatigue data from five sources<sup>19,22-25</sup> for type 304 stainless steel at 21°C (70°F), 538°C (1000°F) to 566°C (1050°F), and 649°C (1200°F) with a strain rate of 0.004 sec<sup>-1</sup>. The parameter values which he obtained are also given in Table 4.

Diercks and Raske<sup>26</sup> have collected low-cycle fatigue data for type 304 stainless steel at elevated temperatures from 10 sources (Refs. 19, 20, 22, 25, 27-32). Included in this listing are the previously unpublished results<sup>29</sup> of three tests each at 538°C (1000°F) and 650°C (1202°F) of specimens from the reference heat 9T2796. These specimens were solution

Table 4. Parameters in Eq. (1), with strain range in percent, for uniaxial low-cycle fatigue of type 304 stainless steel

	Temperature		a <sub>1</sub>	a <sub>2</sub>	a <sub>3</sub>	a <sub>4</sub>	Scatter Factor
	°C	°F					
Code Case 1592-7	38	100	-0.11694	-0.49671	0.8733	13.2130	1.014
Fatigue Design Curves <sup>13</sup>	538-649	1000-1200	-0.12629	-0.58757	0.6105	9.8404	1.021
Code Curves Shifted*	38	100	-0.03258	-0.49894	0.4939	64.3311	1.029
	538-649	1000-1200	-0.06032	-0.60270	0.4788	67.5449	1.022
Code Curves Shifted*	38	100	-0.05555	-0.55565	0.7516	89.0054	1.038
	538-649	1000-1200			0.4194	50.5178	
Average Data <sup>21</sup>	21	70	-0.303	-0.403	5.0	24.7	
	538-566	1000-1050	-0.149	-0.515	1.18	46.77	
	649	1200	-0.151	-0.506	1.04	36.31	

\*Up by a factor of 2 or to the right by a factor of 20, whichever results in a larger value of strain range.

annealed and aged 1000 hours at 593°C (1100°F), and tested at a constant strain rate of 0.004 sec<sup>-1</sup> (slightly greater than the minimum average equivalent strain rate of the present tests). These results are given in Table 5.

Table 5. Uniaxial low-cycle fatigue data<sup>29</sup> for the reference heat (9T2796) of type 304 stainless steel, annealed and aged 1000 hr at 593°C (1100°F)

$\Delta\epsilon_z$ (%)	$N_f$ (cycles)	$\Delta\epsilon_z^p$ (%)	$\Delta\epsilon_z^e$ (%)	$\dot{\epsilon}_z$ sec <sup>-1</sup>	$\frac{\Delta\epsilon_z^e}{\Delta\epsilon_z}$	$F_e$	$\frac{\Delta\epsilon_{equiv}}{\Delta\epsilon_z}$
[538°C (1000°F)]							
2.01	1100	1.57	0.44	0.004	0.219	0.914	0.971
0.99	4951	0.66	0.33	0.004	0.333	0.870	0.957
0.64	15416	0.39	0.25	0.0043	0.391	0.847	0.949
[650°C (1202°F)]							
1.98	722	1.59	0.39	0.004	0.197	0.926	0.975
0.99	2604	0.68	0.31	0.004	0.313	0.883	0.961
0.49	25771	0.27	0.22	0.0039	0.449	0.832	0.944

The pure tension or  $R = 0$  data of Table 1 are plotted in Fig. 5 for all three temperatures employed in this investigation. Also shown are the available 538°C (1000°F) and 650°C (1202°F) data<sup>29</sup> from Argonne National Laboratory for the reference heat in the aged condition, including data for slower strain rates than those listed in Table 5. The three solid-line curves in Fig. 5 represent fits to the present data. The three curves drawn with alternating long and short dashes are average in the sense that they represent fits<sup>21</sup> to data from several sources.<sup>19,22-25</sup> The two remaining dashed-line curves are reconstructions of the average fatigue curves which served as the basis for the Code design curves. The lower of these two curves is based primarily on 649°C (1200°F) data, but the then available 538°C (1000°F) data were not

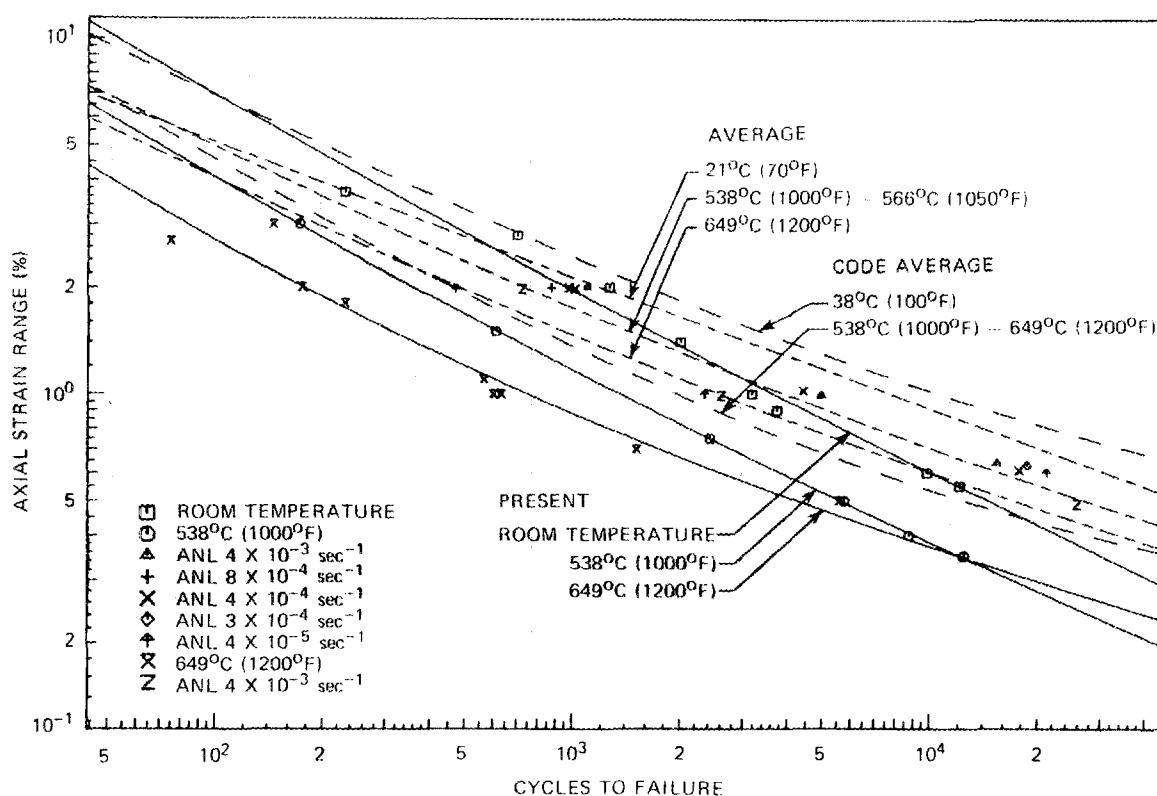


Fig. 5. Uniaxial low-cycle fatigue tests on annealed type 304 stainless steel (heat 9T2796) at room temperature, 538°C (1000°F), and 649°C (1200°F). Constant strain rate data<sup>29</sup> at 538°C (1000°F) and 650°C (1202°F) from Argonne National Laboratory [(same heat, aged 1000 hr at 593°C (1100°F))] is also shown. In each of the present tests, the average strain rate in  $\text{sec}^{-1}$  was equal to the strain range in percent divided by 120.

sufficiently different to require separate treatment.<sup>14</sup> All eight curves were generated using Eq. (1) with the temperature-dependent exponents and coefficients listed in Tables 3 and 4.

The two sets of dashed (or average) curves in Fig. 5 agree reasonably well, except perhaps at low numbers of cycles. The ANL data<sup>29</sup> for both temperatures at  $0.004 \text{ sec}^{-1}$  strain rate lie for the most part slightly above the corresponding average curves. The remaining ANL data at 538°C (1000°F), except for the three points nearest to 20,000 cycles, are in agreement with the usual observation that lowering the strain rate lowers the number of cycles to failure at elevated temperature.

The present data and fitted curves lie for the most part well below the corresponding average curves, despite the effect that the higher average equivalent strain rates at the higher strain ranges should have on the elevated temperature results. The reason for this difference is not known, however there is no reason valid comparisons cannot be made, based on the present data, between results of tests at different ratios of engineering shear strain to axial strain.

### EQUIVALENT STRAIN RANGE

In cylindrical coordinates the equivalent total strain range of Ref. 1 is given by

$$\Delta\epsilon_{\text{equiv}} = \frac{\sqrt{2}}{3} \{(\Delta\epsilon_r - \Delta\epsilon_\theta)^2 + (\Delta\epsilon_\theta - \Delta\epsilon_z)^2 + (\Delta\epsilon_z - \Delta\epsilon_r)^2 + \frac{3}{2} [(\Delta\gamma_{r\theta})^2 + (\Delta\gamma_{\theta z})^2 + (\Delta\gamma_{zr})^2]\}^{1/2}. \quad (3)$$

This form is related to the engineering shear strain range on the octahedral plane (the plane for which the angle between its normal and each of the three principal strain range directions is the same) by  $\Delta\epsilon_{\text{equiv}} = \Delta\gamma_{\text{oct}}/\sqrt{2}$ . An analagous form, used in plasticity theory, is usually restricted to the plastic portion of the strain increments.

In the present experiments  $\Delta\gamma_{r\theta}$  and  $\Delta\gamma_{zr}$  were zero and  $\Delta\epsilon_z$  and  $\Delta\gamma_{\theta z}$  were measured indirectly. The two remaining strain range components were taken to be

$$\Delta\epsilon_r = \Delta\epsilon_\theta = -\nu\Delta\epsilon_z^e - \frac{1}{2}(\Delta\epsilon_z - \Delta\epsilon_z^e) = -\frac{1}{2}\Delta\epsilon_z F_e,$$

where  $\nu$  is Poisson's ratio,  $\Delta\epsilon_z^e$  is the elastic portion of the total axial strain range  $\Delta\epsilon_z$ , and

$$F_e = 1 - (1-2\nu)(\Delta\epsilon_z^e/\Delta\epsilon_z)$$

is a factor that accounts for the effect of elastic strain. Equation

(3) becomes

$$\Delta\epsilon_{\text{equiv}} = \frac{\sqrt{2}}{3} \left[ 2\left(1 + \frac{1}{2} F_e\right)^2 (\Delta\epsilon_z)^2 + \frac{3}{2} (\Delta\gamma_{\theta z})^2 \right]^{1/2} . \quad (4)$$

For a pure torsion test  $\Delta\epsilon_{\text{equiv}} = \Delta\gamma_{\theta z}/\sqrt{3}$  and for a pure tension test  $\Delta\epsilon_{\text{equiv}} = \frac{2}{3} (1 + \frac{1}{2} F_e) \Delta\epsilon_z$ . As  $\Delta\epsilon_z$  increases, the ratio  $\Delta\epsilon_z^e/\Delta\epsilon_z$  ranges from 1 to 0,  $F_e$  from  $2\nu$  to 1, and  $\Delta\epsilon_{\text{equiv}}/\Delta\epsilon_z$  for pure tension from  $\frac{2}{3}(1 + \nu)$  to 1.

For type 304 stainless steel, the minimum value of  $\Delta\epsilon_{\text{equiv}}/\Delta\epsilon_z$  for pure tension is 0.84 at 38°C (100°F), 0.87 at 538°C (1000°F), and 0.88 at 649°C (1200°F), based on values of Poisson's ratio reported in Ref. 33. Taking  $F_e = 1$  or  $\nu = \frac{1}{2}$  (incompressible material) will result in  $\Delta\epsilon_{\text{equiv}}$  being overestimated by at most 19% for type 304 stainless steel, with the error decreasing as temperature,  $\Delta\epsilon_z$ , and  $\Delta\gamma_{\theta z}$  increase. For pure torsion, the error is zero. In constructing the Code Case 1592-7 fatigue design curves directly from uniaxial data,<sup>14</sup> the above error was evidently absorbed in the relatively large factors of safety employed.

Some idea of how quickly the ratio  $\Delta\epsilon_{\text{equiv}}/\Delta\epsilon_z$  for pure tension approaches unity as  $\Delta\epsilon_z$  increases can be obtained by studying the available uniaxial low-cycle fatigue data<sup>26</sup> for which both the total strain range and the plastic strain range are given. The calculated values of  $\Delta\epsilon_{\text{equiv}}/\Delta\epsilon_z$  given in Table 5 seem fairly typical. The lowest value calculated, 0.944, for a total strain range of 0.49% at 650°C (1202°F), represents an error of 6%, while the highest, 0.975, for a total strain range of 1.98% at the same temperature, represents an error of 3%.

In Figs. 6, 7, and 8 the data of Tables 1 and 5 are plotted as equivalent strain range [from Eq. (4) with  $F_e = 1$ ] vs cycles to failure for each of the three temperatures employed in this investigation. Also shown are the curves for  $R = 0, 2,$  and  $\infty$ , generated using Eq. (1) with the temperature-dependent exponents and coefficients of Table 3. Each of Figs. 6, 7, and 8 also contains the appropriate equivalent strain range vs design allowable cycles curve (designated CC in the figure) from Ref. 1 and a curve (designated CCS in the figure) obtained by shifting the Code design curve up by a factor of 2 or to the right by a factor of 20, whichever results in a larger value of strain range. The

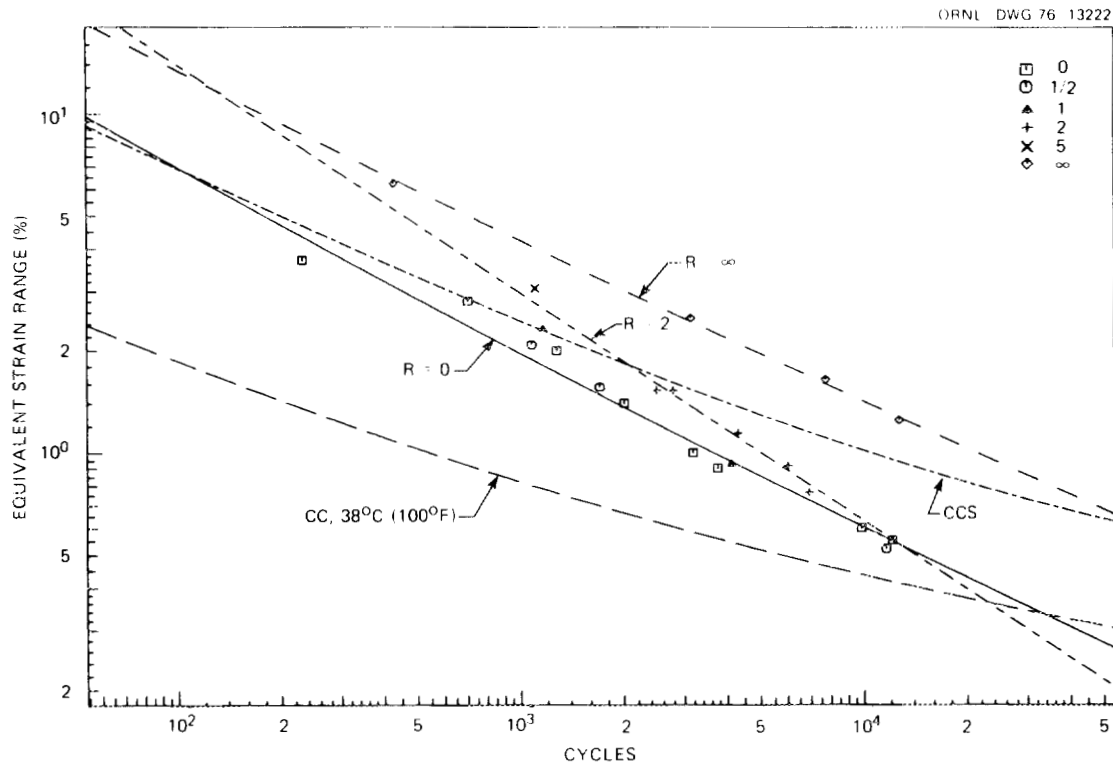


Fig. 6. Equivalent strain range vs cycles to failure in multi-axial low-cycle fatigue tests on annealed type 304 stainless steel (heat 9T2796) at room temperature.

CCS curves are thus representative of the uniaxial data on which the Code design curves are based.<sup>14</sup> The CC and CCS curves were generated using Eq. (1) with the temperature-dependent exponents and coefficients given in Table 4. The CC and CCS curves for 538°C (1000°F) are identical to the curves for 649°C (1200°F), although there are now data available which indicate they should not be.<sup>26</sup>

Several observations can be made regarding Figs. 6, 7, and 8. Firstly, equivalent strain range is not very effective in bringing these low-cycle fatigue data from several multi-axial strain states into coincidence with a common curve. At each temperature, the pure torsion data lie considerably above the pure tension data. The fitted curves also reflect this. Evaluation of the corresponding equations at  $N_f = 1000$  cycles shows that the ratio of equivalent strain range for pure torsion to equivalent strain range for pure tension is 2.15 at room temperature,

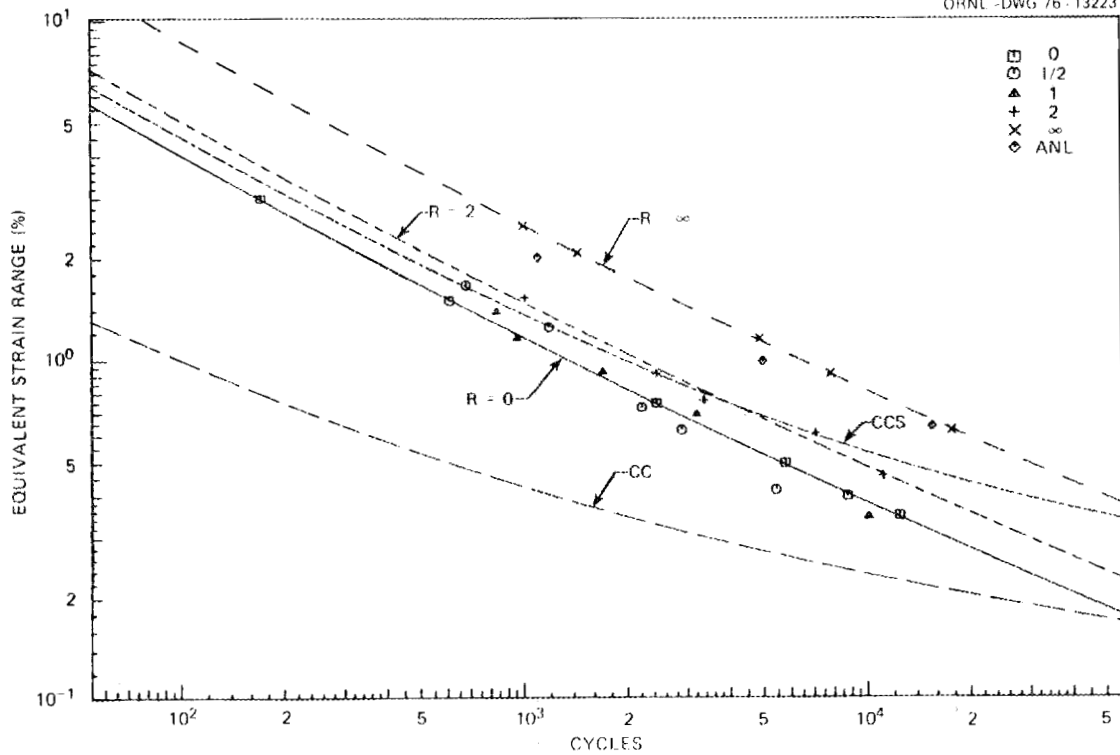


Fig. 7. Equivalent strain range vs cycles to failure in multi-axial low-cycle fatigue tests on annealed type 304 stainless steel (heat 9T2796) at 538°C (1000°F). Uniaxial data<sup>29</sup> from Argonne National Laboratory at a constant strain rate of 0.004 sec<sup>-1</sup> on the same heat in the aged condition is also shown.

2.14 at 538°C (1000°F), and 2.07 at 649°C (1200°F). Similar remarks apply to maximum engineering shear strain range,  $(\Delta\epsilon_1 - \Delta\epsilon_3)$ , and maximum normal strain range,  $\Delta\epsilon_1$ , based on the incompressible equations for the ordered principal strain ranges,  $\Delta\epsilon_1 \geq \Delta\epsilon_2 \geq \Delta\epsilon_3$ , which for combined tension and torsion are given by

$$\Delta\epsilon_1 = \frac{1}{4} \Delta\epsilon_z + \sqrt{\left(\frac{3}{4}\Delta\epsilon_z\right)^2 + \left(\frac{1}{2}\Delta\gamma_{\theta z}\right)^2},$$

$$\Delta\epsilon_2 = -\frac{1}{2}\Delta\epsilon_z, \text{ and} \tag{5}$$

$$\Delta\epsilon_3 = \frac{1}{4}\Delta\epsilon_z - \sqrt{\left(\frac{3}{4}\Delta\epsilon_z\right)^2 + \left(\frac{1}{2}\Delta\gamma_{\theta z}\right)^2}.$$

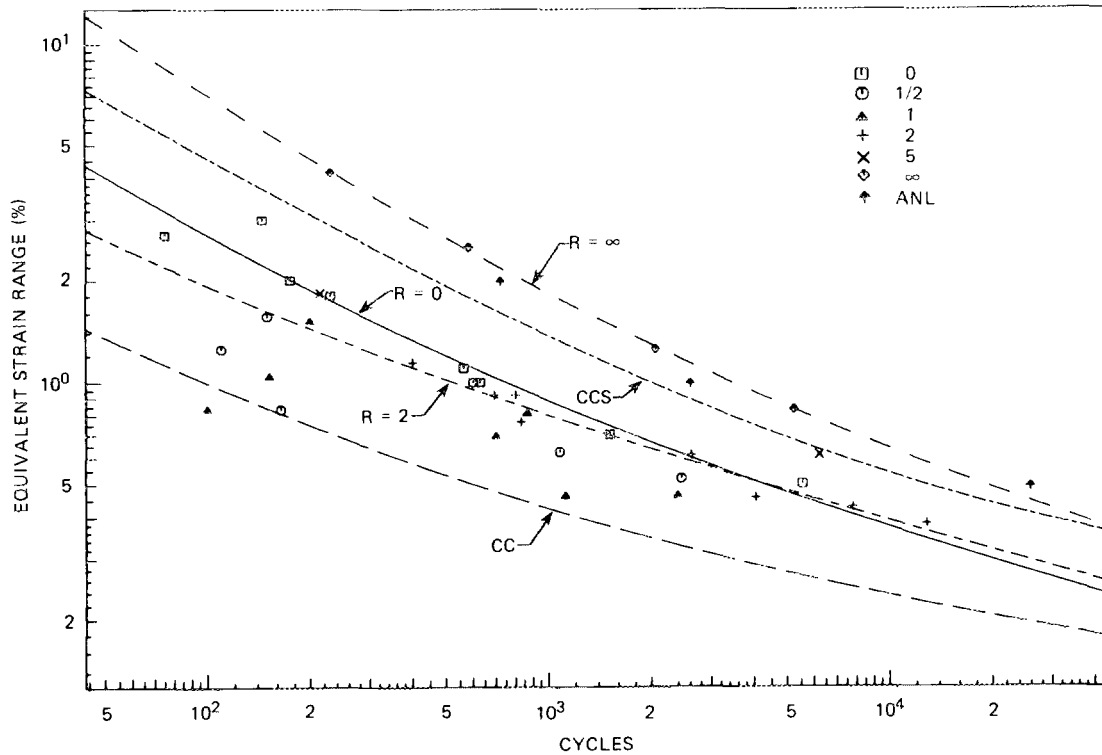


Fig. 8. Equivalent strain range vs cycles to failure in multi-axial low-cycle fatigue tests on annealed type 304 stainless steel (heat 9T2796) at 649°C (1200°F). Uniaxial data<sup>29</sup> from Argonne National Laboratory at 650°C (1202°F) and a constant strain rate of 0.004 sec<sup>-1</sup> on the same heat in the aged condition is also shown.

If maximum engineering shear strain range and maximum normal strain range were plotted vs cycles, figures very similar to Figs. 6, 7, and 8 would result, with relatively small vertical translations of the data points and curves on the log-log coordinates. At 1000 cycles the ratio of maximum shear strain range for pure torsion to maximum shear strain range for pure tension is 2.49 at room temperature, 2.48 at 538°C (1000°F), and 2.39 at 649°C (1200°F). At 1000 cycles the ratio of maximum normal strain range for pure torsion to maximum normal strain range for pure tension is 1.86 at room temperature and at 538°C (1000°F), and 1.79 at 649°C (1200°F).

Secondly, the pure tension data,  $R = 0$ , in Figs. 6, 7, and 8 lie consistently below the CCS curves, while the uniaxial ANL data<sup>29</sup> in

Figs. 7 and 8 lie consistently above. One might reasonably infer from this that all of the present data are lower than average for some unknown reason. There does not seem to be any reason however, to suppose that the apparent influence of multiaxiality has been magnified as a result.

Thirdly, the curves fitted to the present data in Figs. 6 and 7 show less curvature than the CC and CCS curves. If extended far enough beyond the data, these curves will cross the CC or Code design curves at relatively high numbers of cycles, as demonstrated in the figures. This is apparently due to the limited range of fatigue lives in the present data. Not counting the single test at room temperature with  $R = 5$ , the ratio of maximum to minimum cycles for a given test condition ranges from 2.8 for the tests at room temperature with  $R = 2$  to 74 for the tests at  $649^{\circ}\text{C}$  ( $1200^{\circ}\text{F}$ ) with  $R = 0$ . The longest test was 17,600 cycles to failure at  $538^{\circ}\text{C}$  ( $1000^{\circ}\text{F}$ ) with  $R = \infty$  and  $\Delta\gamma_{\theta z} = 1.08\%$ . In addition to lack of curvature, limited range and a limited number of data points permit experimental scatter to have a large influence on the slope of a fitted curve, as is apparently the case for  $R = 2$  in Fig. 6.

Fourthly, there is an inconsistency between the results in Figs. 6 and 7 and the results in Fig. 8. At room temperature and at  $538^{\circ}\text{C}$  ( $1000^{\circ}\text{F}$ ) the pure tension or  $R = 0$  curve comes close to being a lower bound for all of the multiaxial data. It would follow from this that the Code design curves are based on the worst case as far as multiaxiality is concerned. At  $649^{\circ}\text{C}$  ( $1200^{\circ}\text{F}$ ) however, most of the multiaxial data lie below the  $R = 0$  curve. Unfortunately, there is also considerable scatter present in the data for  $R = \frac{1}{2}$  and  $R = 1$  at this temperature, making interpretation of the results more difficult. In fact one of the data points for  $R = 1$  (100 cycles) lies below the Code design curve, although the fitted equivalent strain range curve for this ratio does not cross the design curve in the range of the data. (The nearest crossing is at 42 cycles.)

## PLANE OF MAXIMUM SHEAR STRAIN

Brown and Miller<sup>34</sup> examined multiaxial low and high-cycle fatigue data for many materials and test conditions at room temperature and concluded that the physical quantities which govern fatigue life are the shear and normal strains acting on the plane of maximum shear strain. A similar conclusion in terms of stresses was reached earlier by Findley<sup>35</sup> for high-cycle fatigue. Recent work of Kanazawa and Brown<sup>36</sup> involving out-of-phase combined axial and torsional loading lends further support to this approach. Figures 9, 10, and 11 are plots of normal strain range,  $\Delta\epsilon_{ms} = \frac{1}{2}(\Delta\epsilon_1 + \Delta\epsilon_3)$ , vs one-half the engineering shear strain

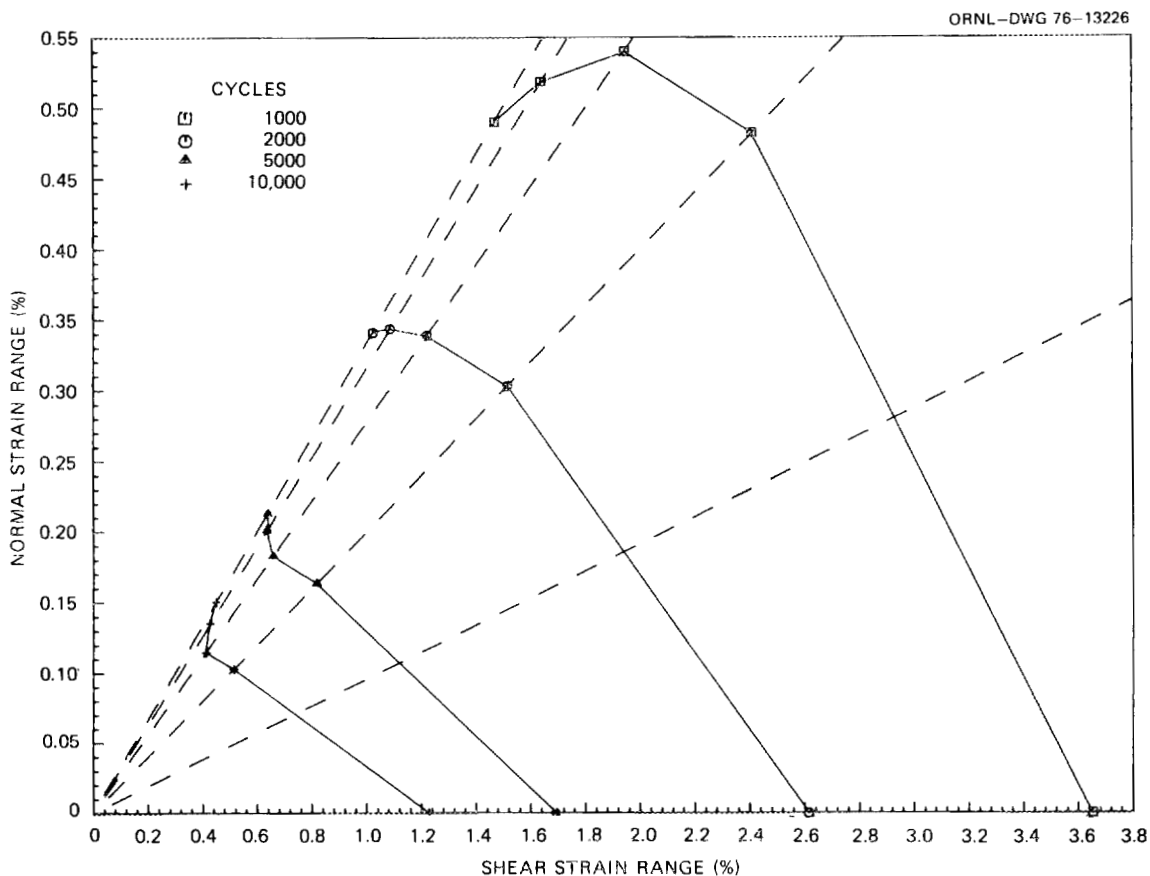


Fig. 9. Constant life contours of normal strain range vs shear strain range on the plane of maximum shear strain for type 304 stainless steel (heat 9T2796) at room temperature.

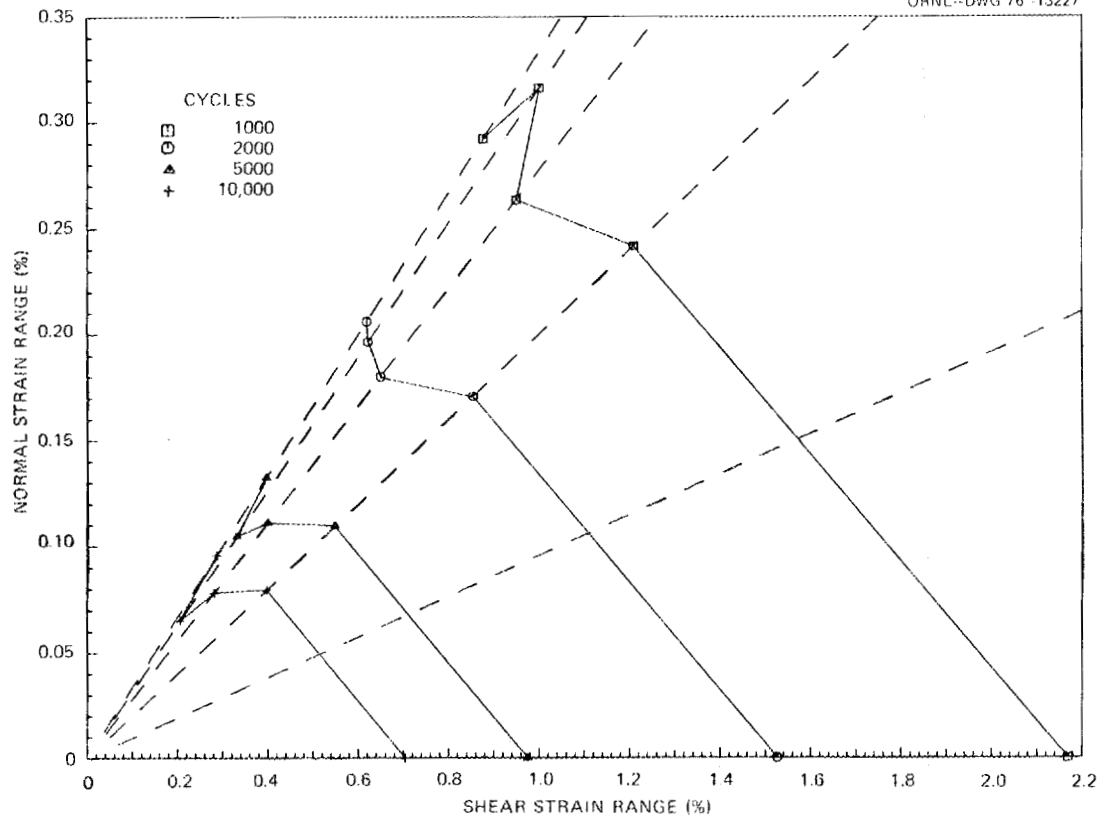


Fig. 10. Constant life contours of normal strain range vs shear strain range on the plane of maximum shear strain for type 304 stainless steel (heat 9T2796) at 538°C (1000°F).

range,  $\frac{1}{2}\Delta\gamma_{ms} = \frac{1}{2}(\Delta\epsilon_1 - \Delta\epsilon_3)$ , on the plane of maximum shear strain range, for 4 values of the number of cycles to failure,  $N_f$ , covering approximately the range of the present data at room temperature, 538°C (1000°F), and 649°C (1200°F) respectively. For combined tension and torsion,

$$\Delta\epsilon_{ms} = \frac{1}{4}\Delta\epsilon_z, \text{ and}$$

$$\frac{1}{2}\Delta\gamma_{ms} = \sqrt{\left(\frac{3}{4}\Delta\epsilon_z\right)^2 + \left(\frac{1}{2}\Delta\gamma_{\theta z}\right)^2},$$

from Eq. (5). The calculations were based on Eq. (1) with the parameters from Table 3 (exponents depending on temperature and coefficients depending on temperature and the ratio,  $R$ , of engineering shear strain

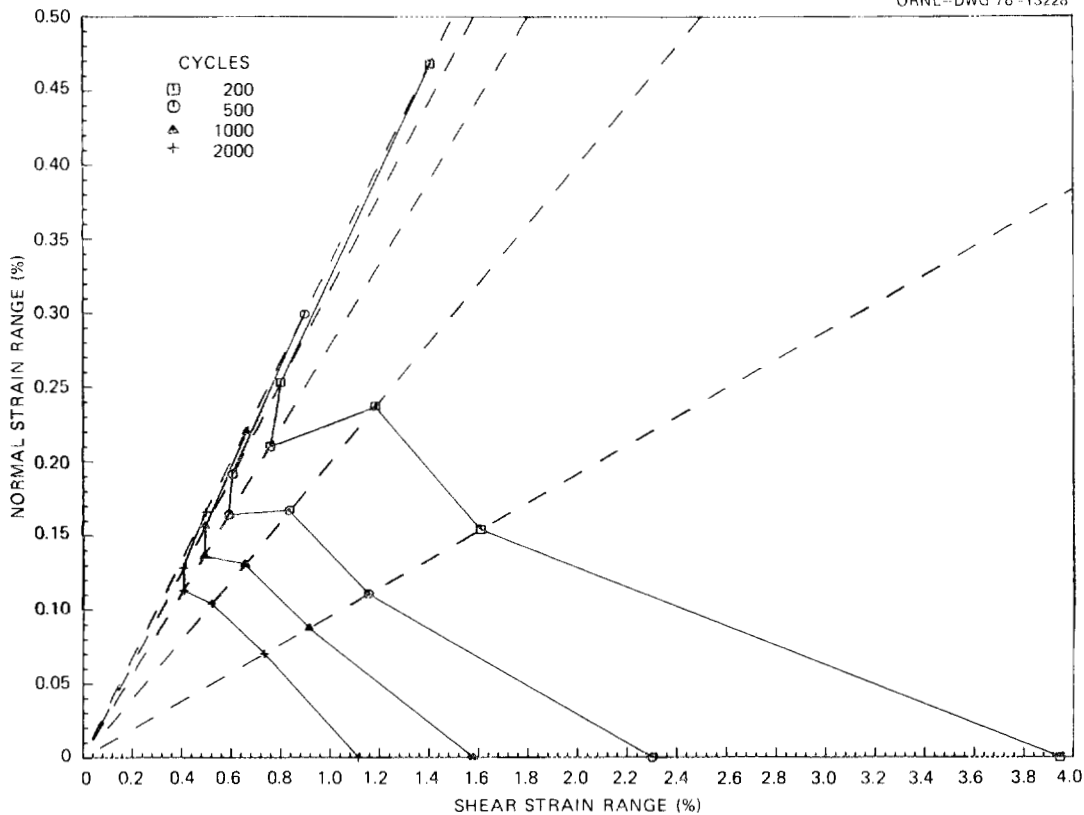


Fig. 11. Constant life contours of normal strain range vs shear strain range on the plane of maximum shear strain for type 304 stainless steel (heat 9T2796) at 649°C (1200°F).

to axial strain). The dashed lines in Figs. 9, 10, and 11 connect points with the same value of  $R$ , and the solid lines connect points with the same value of  $N_f$ . Note that the values of  $N_f$  chosen for 649°C (1200°F) are different from the values chosen for room temperature and 538°C (1000°F). The constant life contours in Fig. 9 are quite smooth, unlike those in Figs. 10 and 11. In any case, the shapes are accurate reflections of the fits to the data, and are therefore subject to the same problems: limited range and limited number of data points, experimental scatter, and apparent inconsistencies as discussed in the previous section. Figures 9, 10, and 11 nevertheless suggest that an effective method of design for multiaxial low-cycle fatigue could be based on the shear and normal strains acting on the plane of maximum shear strain. The type of problem envisioned would reduce to the

determination of the coordinates in  $\Delta\epsilon_{ms}$  vs  $\frac{1}{2}\Delta\gamma_{ms}$  space of the point of intersection of a given radial line with a given constant life contour. If adequate multiaxial data are available to generate reasonably smooth contours, no matter what their shape, linear interpolation between known points on a contour could be used. For example, suppose that the ratio of  $\Delta\epsilon_{ms}$  to  $\frac{1}{2}\Delta\gamma_{ms}$  is 0.0958 and the values of  $\Delta\epsilon_{ms}$  and  $\frac{1}{2}\Delta\gamma_{ms}$  expected to cause failure in 1100 cycles at room temperature are needed. For combined tension and torsion, this corresponds to the single test in Table 1 at  $R = 5$ . The equation of the straight line approximating this portion of the 1100 cycle room temperature contour is

$$\Delta\epsilon_{ms} = -0.369\left(\frac{1}{2}\Delta\gamma_{ms}\right) + 1.29 ,$$

with strain ranges in percent. Intersection with the radial line defined by the above ratio occurs at  $\Delta\epsilon_{ms} = 0.265\%$  and  $\frac{1}{2}\Delta\gamma_{ms} = 2.77\%$ . For combined tension and torsion with  $R = 5$ , this corresponds to an axial strain range,  $\Delta\epsilon_z$ , of 1.06%. In the test referred to above,  $\Delta\epsilon_z$  was 1.00%.

Another possibility is suggested by the shape of the constant life contours in Figs. 9 and 10, namely that they might be approximated by a single straight line connecting the pure tension result with the pure torsion result. The equation for this line is

$$\Delta\epsilon_{ms} = \left(\frac{1}{2}\Delta\gamma_0 - \frac{1}{2}\Delta\gamma_{ms}\right) / \left(2\frac{\Delta\gamma_0}{\Delta\epsilon_0} - 3\right) , \quad (6)$$

where  $\Delta\epsilon_0$  and  $\Delta\gamma_0$  are the strain ranges in pure tension and pure torsion, respectively, and depend on  $N_f$  in accordance with Eq. (1). For combined tension and torsion Eq. (6) reduces to

$$\Delta\epsilon_z = \Delta\epsilon_0 / \left[ \left( \sqrt{\frac{9}{4} + R^2} - \frac{3}{2} \frac{\Delta\epsilon_0}{\Delta\gamma_0} + 1 \right) \right] ,$$

where  $R = \Delta\gamma_{\theta z} / \Delta\epsilon_z$ .

## CUMULATIVE DAMAGE

For the 45 multiaxial, low-cycle fatigue tests listed in Table 2 which were conducted under a sequence of two constant strain ranges, the linear cumulative damage rule (after Palmgren,<sup>37</sup> Langer,<sup>38</sup> and Minor<sup>39</sup>) employed in Ref. 1 reduces to

$$\frac{n_1}{N_1} + \frac{n_2}{N_2} = 1 , \quad (7)$$

where  $n_1$  and  $n_2$  are the numbers of cycles applied at the first and second strain ranges respectively, and  $N_1$  and  $N_2$  are estimates of the number of cycles to failure  $N_f$  for the corresponding single strain range conditions. Note that in all but two cases the strain range sequence was high-low. Two sets of  $N_f$  estimates are given in Table 2. The first is based on the solution of Eq. (1) (with exponents depending on temperature and coefficients depending on temperature and R ratio) for the applied multiaxial strain ranges. With these estimates, the second life fraction,  $n_2/N_2$ , is plotted against the first,  $n_1/N_1$ , in Fig. 12, along with the straight line representing Eq. (7). Many of the data sets in this figure, while remarkably linear in themselves, do not conform to the straight line shown. The most striking example of this is the series of tests at 649°C (1200°F) under a high-low sequence of straining with  $R = 1$ . One possibility is that the estimates of  $N_f$  based on the constant strain range tests at 649°C (1200°F) are unreliable. If so, this is another example of the apparent lack of consistency pointed out earlier in the constant strain range, multiaxial data at this temperature.

To explore this possibility further, a second set of  $N_f$  estimates as given in Table 2 were made by fitting straight lines to the  $n_2$  vs  $n_1$  data in the high-low tests by the method of least squares. For the two cases in which a low-high sequence was used, the 1-2 sequence designations were interchanged and the data were incorporated into the corresponding high-low data sets in order to have common estimates of  $N_f$  for the same straining and temperature conditions. The resulting best-fit life fractions are plotted in Fig. 13.

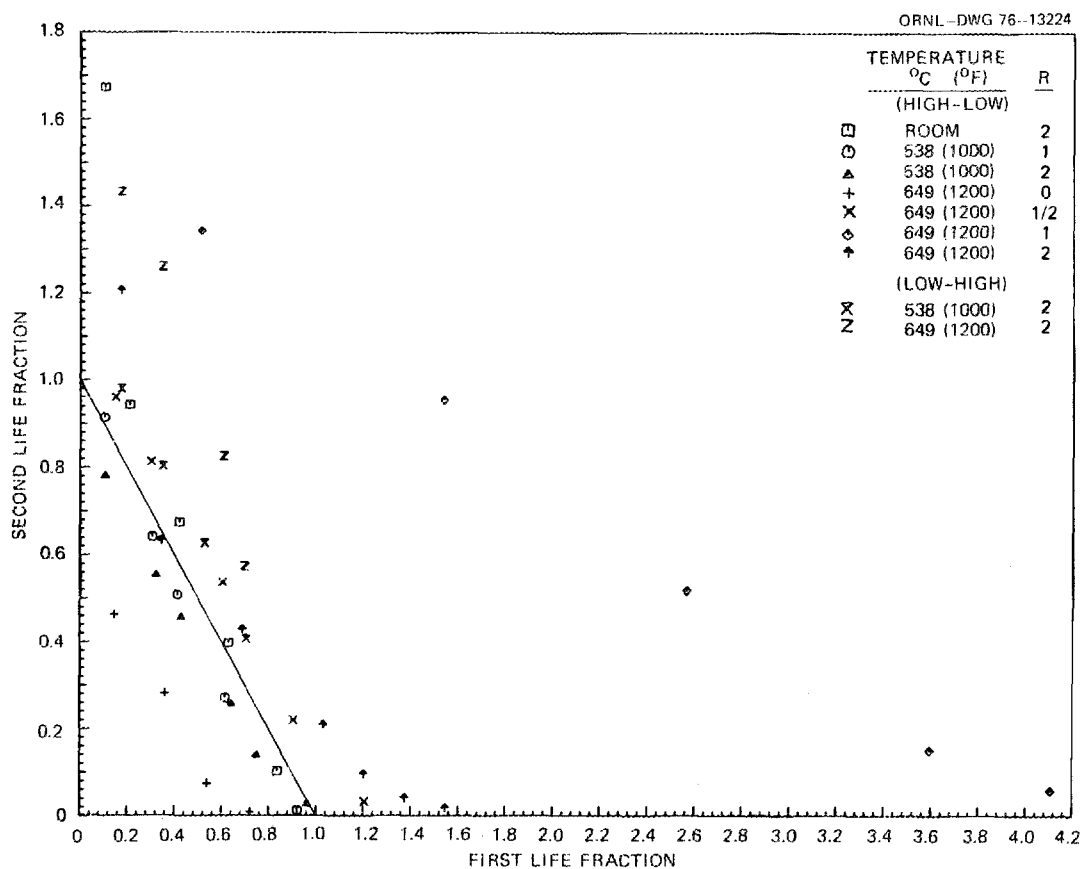


Fig. 12. Two-part multiaxial cumulative damage tests on type 304 stainless steel (heat 9T2796) at room temperature, 538°C (1000°F), and 649°C (1200°F), with engineering shear strain to axial strain ratios of 0, 1/2, 1, and 2, and with high-to-low and low-to-high strain range sequences.

The improved agreement with Eq. (7) of the data in Fig. 13 as compared with that in Fig. 12 is both obvious and expected, but there remains considerable question as to how meaningful these results are. It is reassuring to note that most of the data points which lie significantly above the straight line in Fig. 13 are from tests in which a low-high sequence of straining was followed while all points below the line are from high-low tests. This distinction, which is not as clear in Fig. 12, conforms to the sequence effect usually reported<sup>22</sup> in such tests.

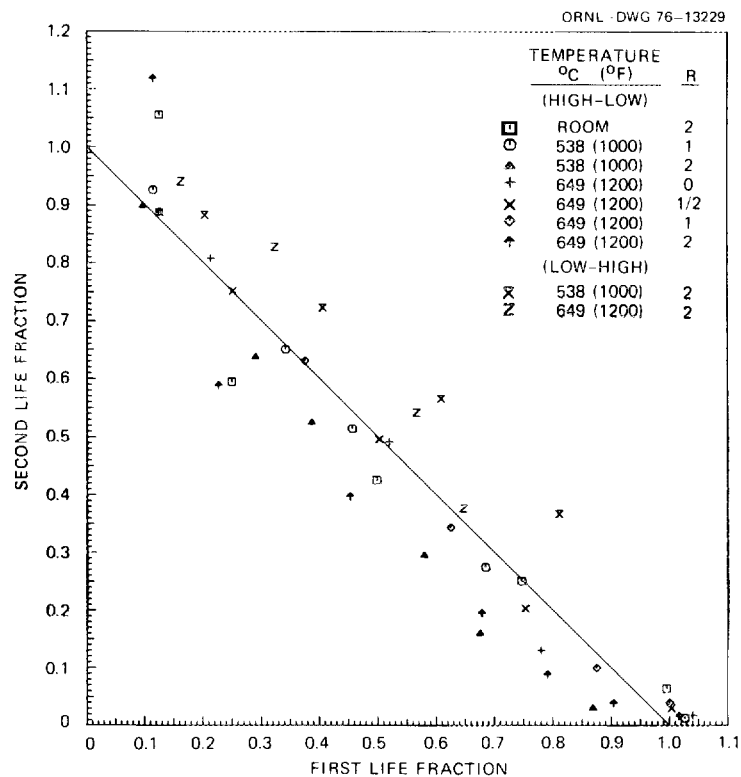


Fig. 13. Two-part multi-axial cumulative damage data of Fig. 12 with  $N_f$  values chosen from fit to linear cumulative damage law.

Despite the unorthodox treatment of the data plotted in Fig. 13 it may be more faithful to the underlying multi-axial cumulative damage behavior of this material than is Fig. 12. Hopefully, additional data will become available as more attention is focused on multi-axial low-cycle fatigue.

#### SUMMARY AND CONCLUSIONS

Current fatigue design methods are based on: (1) a definition of equivalent strain range, (2) a linear cumulative damage rule, and (3) a temperature and material dependent relationship between equivalent strain range and allowable cycles of straining. The results presented here are relevant to an assessment of the effectiveness of each of these

basic elements, but are specific to type 304 stainless steel. With regard to (1), these results show that the current definition of equivalent strain range is not a very effective criterion for accounting for the influence of multiaxial loading on fatigue. The same observation applies to two other traditional measures, the maximum shear strain range and the maximum principal strain range. However, the results at room temperature and 538°C (1000°F) indicate that on an equivalent strain basis uniaxial stressing is the most detrimental fatigue loading condition of those investigated. Since the relationship in (3) above is based on this condition, current methods might therefore be characterized as conservative with respect to multiaxiality. The results at 649°C (1200°F) do not support this position, but do not themselves constitute a convincing counter example.

Concerning (2), these results do not indicate that multiaxial loading is significantly different from uniaxial loading with regard to the effectiveness of a linear cumulative damage rule.

These results also indicate that a fatigue failure criterion based on the shear and normal strains acting on the plane of maximum shear strain would be more effective than criteria based on the other measures considered. Additional multiaxial testing, especially at elevated temperatures, is needed to guide further development of such a criterion.

#### ACKNOWLEDGMENT

The experiments were performed by O. G. Bilir, Research Assistant, The Pennsylvania State University.

## REFERENCES

1. "Case 1592-7," *Cases of ASME Boiler and Pressure Vessel Code*, American Society of Mechanical Engineers, New York, December 1975.
2. S. Y. Zamrik, *The Effect of Biaxiality in Creep-Fatigue at Elevated Temperatures*, ORNL/Sub-3649-3, Pennsylvania State University, March 1975.
3. H. E. McCoy, Jr., and R. D. Waddell, Jr., "Mechanical Properties of Several Products from a Single Heat of Type 304 Stainless Steel," *Transactions, American Society of Mechanical Engineers, Journal of Engineering Materials and Technology*, Vol. 97, No. 4, 1976, pp. 343-349.
4. R. W. Swindeman, W. J. McAfee, and V. K. Sikka, "Product Form Variability in the Mechanical Behavior of Type 304 Stainless Steel at Room Temperature and 593°C (1100°F)," *Symposium on Reproducibility and Accuracy of Mechanical Tests*, American Society for Testing and Materials, May 1976.
5. O. H. Basquin, "The Exponential Law of Endurance Tests," *Proceedings, American Society for Testing and Materials*, Vol. 11, 1910, pp. 625-630.
6. L. F. Coffin, Jr., "A Study of the Effects of Cyclic Thermal Stresses on a Ductile Metal," *Transactions, American Society of Mechanical Engineers*, Vol. 76, 1954, pp. 931-950.
7. L. F. Coffin, Jr., "Fatigue at High Temperature-Prediction and Interpretation," *Proceedings, Institution of Mechanical Engineers*, Vol. 188, 1974, pp. 109-127.
8. S. S. Manson, *Behavior of Materials Under Conditions of Thermal Stress*, NACA TN-2933, National Advisory Committee for Aeronautics, 1953.
9. S. S. Manson, "Fatigue: A Complex Subject-Some Simple Approximations," *Experimental Mechanics*, Vol. 5, No. 7, 1965, pp. 193-226.
10. J. D. Morrow, "Cyclic Plastic Strain Energy and Fatigue of Metals," *Internal Friction, Damping and Cyclic Plasticity*, ASTM STP 378, American Society for Testing and Materials, 1965, pp. 45-87.
11. *Computer Subroutine Libraries in Mathematics and Statistics*, IMSL LIB-0005, International Mathematical and Statistical Libraries, Houston, 1975.
12. K. M. Brown, *Derivative Free Analogues of the Levenberg-Marquardt and Gauss Algorithms for Nonlinear Least Squares Approximations*, Technical Report No. 320-2994, IBM Philadelphia Scientific Center, 1970.

13. W. J. McAfee, T. W. Pickel, and W. K. Sartory, "Core Structures Design Criteria and Data," *High-Temperature Structural Design Methods for LMFBR Components Progress Report for Period Ending Dec. 31, 1973*, ORNL-4947, Oak Ridge National Laboratory, pp. 197-215.
14. "Criteria for Design of Elevated Temperature Class 1 Components in Section III, Division 1, of the ASME Boiler and Pressure Vessel Code," American Society of Mechanical Engineers, May 1976.
15. J. B. Conway, *An Analysis of the Relaxation Behavior of AISI 304 and 316 Stainless Steel at Elevated Temperatures*, GEMP-730, General Electric Nuclear Systems Programs, December 1969.
16. J. T. Berling and J. B. Conway, "Effect of Hold Time on the Low Cycle Fatigue Resistance of 304 Stainless Steel at 1200°F, Part II, Materials and Fabrication," *First International Conference on Pressure Vessel Technology*, American Society of Mechanical Engineers, 1970.
17. J. T. Berling and T. Slot, "Effects of Temperature and Strain Rate on Low Cycle Fatigue Resistance of AISI 304, 316, and 348 Stainless Steels," *Fatigue at High Temperatures*, ASTM STP 459, American Society for Testing and Materials, 1970, pp. 3-30.
18. J. B. Conway, *Evaluation of Plastic Fatigue Properties of Heat-Resistant Alloys*, GEMP-740, General Electric Nuclear Systems Programs, December 1969.
19. C. E. Jaske, H. Mindlin, and J. S. Perrin, "Low-Cycle-Fatigue Evaluation of Reactor Materials," *Progress on LMFBR Cladding, Structural, and Component Materials Studies During July 1970 through June 1971, Annual Report Task 32, Final Report Task 14*, BMI-1914, Battelle-Columbus Laboratories, July 1971, pp. A2-A44.
20. C. E. Brinkman, G. E. Korth, and J. M. Beeston, "Influence of Irradiation on the Creep-Fatigue Behavior of Several Austenitic Stainless Steels and Incoloy 800 at 700°C," *Effects of Radiation on Substructure and Mechanical Properties of Metals and Alloys*, ASTM STP 529, American Society for Testing and Materials, 1973, pp. 473-492.
21. J. P. Strizak, "Fatigue-Life Testing," *Mechanical Properties Test Data for Structural Materials Quarterly Progress Report for Period Ending April 30, 1976*, ORNL-5150, Oak Ridge National Laboratory, pp. 192-205.
22. J. B. Conway, R. H. Stentz, and J. T. Berling, *Fatigue, Tensile, and Relaxation Behavior of Stainless Steels*, TID-26135, United States Atomic Energy Commission, 1975.

23. C. E. Jaske, H. Mindlin, and J. S. Perrin, "Low-Cycle-Fatigue Evaluation of Reactor Materials," *Progress on LMFBR Cladding, Structural, and Component Materials Studies During July 1971 through June 1972, Final Report, Task 32*, BMI-1928, Battelle-Columbus Laboratories, July 1972.
24. D. R. Diercks, Argonne National Laboratory, personal communication with J. P. Strizak, January 1976.
25. C. R. Brinkman and G. E. Korth, *Heat-to-Heat Variations in the Fatigue and Creep-Fatigue Behavior of AISI Type 304 Stainless Steel, and the Fatigue Behavior of Type 308 Stainless Steel Weld Materials*, ANCR-1097, Aerojet Nuclear Co., May 1973.
26. D. R. Diercks and D. T. Raske, "Statistical Analysis and Regression Fit of Elevated-Temperature Low-Cycle Fatigue Data on Type 304 Stainless Steel," *ibid.* Ref. 21, pp. 3-34.
27. R. W. Weeks, D. R. Diercks, and C. F. Cheng, *ANL Low-Cycle Fatigue Studies - Program, Results, and Analysis*, ANL-8009, Argonne National Laboratory, November 1973.
28. D. R. Diercks, "Statistical Analysis of Low-Cycle Fatigue Data Scatter," *Mechanical Properties Test Data for Structural Materials Quarterly Progress Report for Period Ending July 31, 1975*, ORNL-5106, Oak Ridge National Laboratory.
29. D. R. Diercks, P. S. Maiya, and S. Majumdar, Argonne National Laboratory, previously unpublished data included in Ref. 26.
30. G. D. Korth and M. D. Harper, *Effects of Neutron Radiation on the Fatigue and Creep/Fatigue Behavior of Type 304 Stainless Steel Weld Metal at Elevated Temperature*, ASTM STP 570, American Society for Testing and Materials, 1975.
31. G. E. Korth and M. D. Harper, *Semi-Annual Progress Report, Irradiation Effects on Reactor Structural Materials, August 1973-January 1974*, HEDL-TME-74-9, Hanford Engineering Development Laboratory, p. ANC-4.
32. G. E. Korth and M. D. Harper, "Fatigue Tests on Cladding and Structural Materials," *Mechanical Properties Test Data for Structural Materials Quarterly Progress Report for Period Ending Oct. 31, 1974*, ORNL-5103, Oak Ridge National Laboratory.
33. *Nuclear Systems Materials Handbook*, TID-26666, Hanford Engineering Development Laboratory, Group 1, Section 2, Mar. 15, 1971.
34. M. W. Brown and K. J. Miller, "A Theory for Fatigue Failure Under Multiaxial Stress-Strain Conditions," *Proceedings, Institution of Mechanical Engineers*, Vol. 187, 1973, pp. 745-755.

35. W. N. Findley, *Combined Stress Fatigue Strength of 76S-T61 Aluminum Alloy with Superimposed Mean Stresses and Corrections for Yielding*, NACA TN-2924, National Advisory Committee for Aeronautics, May 1953.
36. K. Kanazawa and N. W. Brown, "Low-Cycle Fatigue Under Out-of-Phase Combined Axial and Torsional Loads," *Second International Conference on Mechanical Behavior of Materials*, Boston, August 1976.
37. A. Palmgren, "Die Lebensdauer von Kugellagern," ("The Life of Ball Bearings"), *Zeitschrift des Vereins Deutscher Ingenieure*, Vol. 68, No. 14, 1924, pp. 339-341.
38. B. F. Langer, "Fatigue Failure from Stress Cycles of Varying Amplitude," *Transactions, American Society of Mechanical Engineers*, Ser. A, Vol. 59, 1937, pp. A160-A162.
39. M. A. Miner, "Cumulative Damage in Fatigue," *Journal of Applied Mechanics* Vol. 12, 1945, pp. A159-A164.



ORNL/TM-5609  
Dist. Category  
UC-79, -79e, -79h, -79k

## INTERNAL DISTRIBUTION

- |        |                              |        |                                    |
|--------|------------------------------|--------|------------------------------------|
| 1.     | R. L. Battiste               | 40.    | W. J. McCarthy                     |
| 2-6.   | J. J. Blass                  | 41.    | H. E. McCoy                        |
| 7.     | M. K. Booker                 | 42.    | L. E. McNeese                      |
| 8.     | C. R. Brinkman               | 43.    | J. G. Merkle                       |
| 9.     | J. W. Bryson                 | 44.    | S. E. Moore                        |
| 10.    | J. H. Butler                 | 45.    | E. T. Onat (consultant)            |
| 11.    | J. P. Callahan               | 46.    | P. Patriarca                       |
| 12.    | A. E. Carden (consultant)    | 47.    | H. Postma                          |
| 13.    | J. A. Clinard                | 48-50. | C. E. Pugh                         |
| 14.    | C. W. Collins                | 51.    | M. Richardson                      |
| 15.    | W. E. Cooper                 | 52.    | D. N. Robinson                     |
| 16-18. | J. M. Corum                  | 53.    | G. C. Robinson                     |
| 19.    | W. R. Corwin                 | 54.    | W. K. Sartory                      |
| 20.    | F. L. Culler                 | 55.    | D. Scott                           |
| 21.    | J. R. Ellis                  | 56.    | V. K. Sikka                        |
| 22.    | G. G. Fee                    | 57.    | G. M. Slaughter                    |
| 23.    | W. F. Ferguson               | 58.    | J. E. Smith                        |
| 24.    | W. R. Gall                   | 59.    | I. Spiewak                         |
| 25.    | R. H. Gallagher (consultant) | 60.    | J. P. Strizak                      |
| 26.    | M. J. Goglia                 | 61.    | R. W. Swindeman                    |
| 27.    | W. L. Greenstreet            | 62.    | J. J. Taylor                       |
| 28.    | A. G. Grindell               | 63.    | D. B. Trauger                      |
| 29.    | R. C. Gwaltney               | 64.    | J. R. Weir                         |
| 30.    | W. O. Harms                  | 65.    | G. D. Whitman                      |
| 31.    | H. W. Hoffman                | 66.    | W. J. Wilcox                       |
| 32.    | S. K. Iskander               | 67.    | G. T. Yahr                         |
| 33.    | P. R. Kasten                 | 68.    | H. C. Young                        |
| 34.    | R. T. King                   | 69.    | Patent Office                      |
| 35.    | R. L. Klueh                  | 70-72. | Central Research Library           |
| 36.    | K. C. Liu                    | 73.    | Y-12 Document Reference<br>Section |
| 37.    | R. E. MacPherson             | 74-81. | Laboratory Records Department      |
| 38.    | W. R. Martin                 | 82.    | Laboratory Records (RC)            |
| 39.    | W. J. McAfee                 |        |                                    |

Subcontractors

83. H. Armen, Jr., Grumman Aerospace Corporation, Bethpage, NY 11714
84. R. W. Barsoum, Combustion Engineering, Inc., Windsor, CT 06095
85. L. F. Coffin, General Electric Company, Research and Development Center, P. O. Box 8, Schenectady, NY 12301
86. R. L. Egger, Boeing Company, Aerospace Group, P. O. Box 3999, Seattle, WA 98124
87. C. E. Jaske, Battelle Columbus Laboratories, 505 King Ave., Columbus, OH 43201

- 88. R. I. Jetter, Atomics International, P. O. Box 309, Canoga Park, CA 91304
- 89. S. S. Manson, Case Western Reserve University, Cleveland, OH 44106
- 90. C. C. Schultz, Babcock & Wilcox Company, P. O. Box 835, Alliance, OH 44601
- 91-93. S. Y. Zamrik, Pennsylvania State University, University Park, PA 16802

## EXTERNAL DISTRIBUTION

- 94-95. Director, Division of Reactor Development and Demonstration, U.S. Energy Research and Development Administration, Washington, DC 20545
- 96. Director, Reactor Division, USERDA, ORO
- 97. Research and Technical Support Division, USERDA, ORO
- 98-386. Given distribution as shown in TID-4500 under categories UC-79, -79e, -79h, -79k